# Piezoelectric Lateral-Extensional Mode Resonators with Reconfigurable Electrode and Resonance Mode-Switching Behavior Enabled by a $VO_2$ Thin-Film

Ting Hung Liu, *Student Member, IEEE*, Xu Han, Juan Pastrana, *Student Member, IEEE*, Nelson Sepúlveda, *Senior Member, IEEE*, and Jing Wang, *Senior Member, IEEE*

***Abstract*— This paper presents the first two-port lateral-extensional mode zinc oxide (ZnO) piezoelectric resonator with a reconfigurable bottom electrode that is enabled by embedding a vanadium dioxide ($VO_2$) thin film. The insulator-to-metal phase transition of $VO_2$ is triggered by substrate heating that translates to abrupt changes of electric field patterns and piezoelectrically transduced modal vibrations, thus allowing mode-switching of piezoelectric resonators at specific frequencies. Finite element method (FEM) analysis was employed to model the broadband frequency response, while frequency characteristics of the corresponding two-port resonator were measured over a temperature range between 20°C and 95°C with a specific focus on two resonances at 88 and 148 MHz. By leveraging the hysteretic behavior of $VO_2$ thin film during a heating/cooling cycle, a change of both the capacitive feedthrough and resonance signal levels were observed, due to the abrupt change in the conductivity of $VO_2$ during its phase transition. The unique switch-on behavior of the resonance at 88 MHz starts at 70°C during the heating cycle, while the switch-off transition begins at 60°C during the cooling cycle. On the other hand, when the temperature is increased from 20°C to 60°C, a decrease of the insertion loss and resonance frequency of 12 dB and 0.28 MHz, respectively, were observed for the resonance at 148 MHz. Meanwhile, a resonance frequency increase of 0.42 MHz was observed during a temperature increase from 60°C to 95°C, which can be ascribed to the $VO_2$ phase transition from monoclinic to rutile phase. The hysteresis loops for insertion loss and resonance frequency indicate a different critical temperature for the phase transition from the monoclinic (insulator) phase and rutile (metallic) phase and vice versa. The substantial variation of the temperature coefficient of frequency can be largely ascribed to electrode reconfiguration enabled by $VO_2$ phase transition.**

***Index Terms*—microelectromechanical systems (MEMS), lateral extensional mode, piezoelectric thin film transducers, phase transition material, tunable resonators**

## I. Introduction

Microelectromechanical system (MEMS) resonators have been widely investigated as timing and frequency control devices and sub-systems of radio frequency (RF) front ends, such as, filters, mixers, oscillators, frequency synthesizers in wireless communication systems [1]. The RF MEMS resonator technologies can be divided into two main categories, which are capacitively transduced resonators [2][3] and piezoelectrically transduced resonators. Piezoelectric resonators are typically composed of a piezoelectric thin film that is sandwiched in between patterned top and bottom electrodes that are designed to excite the desired resonance mode through matching the electric field with the strain field of the desired mode shape [4]. The common piezoelectric materials employed by piezoelectric resonators are aluminum nitride (AlN) [5]-[7], lithium niobate ($LiNbO_3$) [8]-[10], zinc oxide (ZnO) [11]-[13], [14] and lead zirconate titanate (PZT) [14]-[16]. The electric field generated by the top and bottom electrode across the piezoelectric transducer layer creates an in-plane lateral strain distribution, which excites the resonator body into modal vibration of the corresponding mode shape and resonance frequency. There are different types of vibration modes in MEMS resonators, such as, flexural mode, shear mode, and extensional mode. There are a few extensional mode types, including length-extensional mode, width-extensional mode, thickness mode, and lateral extensional modes [17]. AlN and ZnO are widely investigated piezoelectric materials that are employed along with inter-digitated (IDT) electrodes for lateral extensional mode resonators [13], [16], [18]-[20], where the resonance frequency

Manuscript received XXXX XX, XXX; revised XXXXXX XX, XXX; accepted XXXXXX XX, XXX. Date of publication XXXXX XX, XXXX; date of current version XXXX XX, XXXX *(Corresponding author: Ting Hung Liu and Jing Wang)*

T. H. Liu is with the Electrical Engineering Department, University of South Florida, Tampa, FL 33620 USA. (e-mail: tinghung@usf.edu)

X. Han was with the Electrical Engineering Department, University of South Florida, Tampa, FL 33620 USA. He is now with Akoustis Technologies, Huntersville, NC 28078 USA (e-mail: nevelonly@gmail.com)

J. Pastrana is with the Department of Electrical and Computer Engineering, Michigan State University, East Lansing, MI 48824 USA (e-mail: pastran3@msu.edu)

N. Sepúlveda is with the Department of Electrical and Computer Engineering, Michigan State University, East Lansing, MI 48824 USA (e-mail: sepulve6@msu.edu).

J. Wang is with the Electrical Engineering Department, University of South Florida, Tampa, FL 33620 USA. (e-mail: jingw@usf.edu).

Color versions of one or more of the figures in this paper are available online at http://ieeexplore.ieee.org.

Digital Object Identifier XXXXXXX.

is proportional to the pitch size of the top IDT electrodes or another characteristic dimension defined by high-resolution lithography. There are many prior works on IDT resonators to cover topics such as anchor losses [21][22], electrode material [23][24], and electrode design [20][25][26]. Recently, the bottom electrode design has also been explored [20][27]-[29] for the purpose of enhancing performance metrics such as quality factor ($Q$), electromechanical coupling ($k_t^2$) and figure of merit (FOM) as well as capacitive feedthrough reduction.

In recent years, significant efforts have been committed to implement high performance piezoelectric MEMS resonators, including devices that have been designed to cope with high demand of reconfigurable functionalities, while mitigating energy dissipations and retaining high qualify factor. For instance, advancements have been made by incorporating chalcogenide phase-change materials (e.g., germanium telluride (GeTe)) into MEMS resonators [30][31]. Its phase transition at approximately 430 °C comes with drastic changes in terms of its resistance (on the order of $10^6$) between the OFF amorphous phase and ON crystalline phase. As a consequence, the ability to cycle between the ON/OFF state over large durations [32], low insertion loss values [3], and resonance frequencies of 3.6 GHz [33] have been reported. Meanwhile, other alternative phase-transition materials, such as vanadium dioxide ($VO_2$), have also been studied that have demonstrated repeatable behavior with reconfigurable and programmable memory states that could be incorporated into a new design of piezoelectric resonators to offer ease of fabrication, low power consumption, and lower transition temperatures.

Vanadium dioxide ($VO_2$) is a phase-change material that exhibits several crystalline phases. At room temperature, $VO_2$ presents itself with a low-temperature monoclinic phase, which transforms reversely to a high-temperature rutile-type structure near 68°C [34]. The insulator-to-metal transition (IMT) of the phase-change material is accompanied by changes in the mechanical [35][36], optical [37][38], and electrical [39] properties. Hysteretic behavior is also anticipated during the phase transition, which has been exploited to demonstrate high-performance MEMS devices with programmable capabilities [38][40]. In the field of MEMS resonators, a thin film $VO_2$ has been deposited on top of the device as a part of the resonator body. During the heating cycle and as a consequence of the IMT, stresses are induced to the resonator body that results in a resonance frequency shift. This shows the potential of the $VO_2$ to offer unique reconfigurability for developing tunable band pass filters or other frequency control and timing functions [41].

In an effort to further contribute solutions in achieving high reliability and reconfigurability, we demonstrate, for the first time, the incorporation of $VO_2$ phase-change material within two-port ZnO piezoelectric lateral-extensional mode resonators with reconfigurable bottom electrodes. The effects of the IMT of $VO_2$ on the electric field patterns between the electrodes are studied. An equivalent circuit model is adopted to offer a clear indication on how the addition of $VO_2$ significantly affects the parasitic capacitance of the device based on equivalent circuit model (e.g., mBVD model), thus translating to a substantial signal response change at the targeted resonance frequencies. In addition, a finite element method (FEM) study is presented that closely agrees with the experimental results and aids in the identification of the specific resonance modes of the resonator.

## II. Reconfigurable Bottom Electrode Design

A 320μm × 80μm thin-film ZnO piezoelectric rectangular-plate lateral-extensional mode resonator with a reconfigurable bottom electrode, which can transform between slot-divided and solid rectangular plate, have been strategically designed and implemented by exploiting the temperature-induced phase transition of a $VO_2$ film. There is one center-located and side-supporting anchor attached on each width side to suspend the resonator plate. The width of each the top electrode IDT finger is 12μm and the gap between two adjacent IDT fingers is 5μm. The width of slot-divided bottom electrode is 5μm, which are aligned with the gaps of the two-port top IDT electrodes. The thickness of each layer is detailed in the fabrication section.

Fig. 1 presents the schematic-view diagram of two ZnO piezoelectric resonators, one with a rectangular-plate bottom electrode with slot-divided fingers (Fig. 1 (a)) and another design with a solid rectangular shaped bottom electrode (Fig. 1 (b)). As shown in Fig. 1(a), the reconfigurable bottom electrode design strategy in this work is original and innovative, which consists of a slot-divided Pt bottom electrode stacked on top of a $VO_2$ film as a phase-change material. Meanwhile, the slot-divided Pt bottom electrode is intentionally positioned and aligned within the gaps of the two-port IDT top electrodes to create a unique mode-switching behavior as shown in Fig. 1.

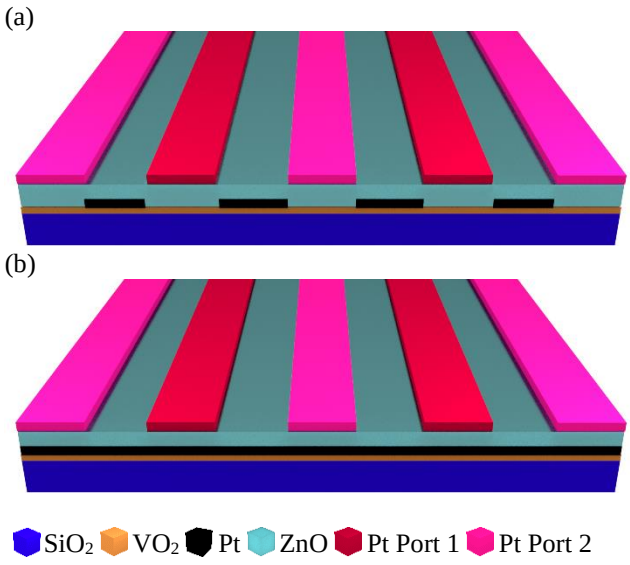


Fig. 1. Schematic-view diagrams of ZnO piezoelectric lateral extensional mode resonators with embedded $VO_2$ phase-transition thin film underneath a Pt electrode: (a) Design with a reconfigurable electrode composed of slot-divided Pt electrode; and (b) Design with a solid Pt electrode.

As shown in Fig. 2, a rectangular-shaped bottom electrode with slot-divided fingers sandwiched between layers of ZnO piezoelectric transducer and phase-transitionable $VO_2$ have been adopted to investigate the patterns of the electric fields generated between the IDT top and reconfigurable bottom electrodes on the modal vibration and piezoelectrically-transduced frequency characteristics. In order to strengthen the

changes of the electric field patterns and modal vibrations, the bottom electrode fingers are strategically designed to be aligned with the gaps of the two-port interdigitated top electrodes without any overlap as shown in Fig. 1 (a). Thus, the electric field and piezoelectric response changes that are induced by the phase transition of the $VO_2$ thin film is maximized. For the pulsed laser deposited (PLD) $VO_2$ film, the monoclinic (insulator) phase to rutile (metallic) phase transition occurs as temperature rises to roughly 68°C. Below 68°C, thin-film $VO_2$ is under monoclinic phase to act as an insulation layer underneath slot-divided Pt bottom electrode. As the temperature rises above 68°C, the thin-film $VO_2$ transitions into rutile phase to behave as a conductive layer to completely fill the divided slots and form a solid rectangular plate, thus reconfiguring the bottom electrode geometry. To the best of our knowledge, $VO_2$ phase-transition material enabled electrode reconfiguration and resonator mode-switching behavior has never been reported before, and this represents a new strategy to reconfigure acoustic resonators after fabrication. Moreover, intriguing hysteresis of resonance responses over temperature range of the $VO_2$ phase transition has been observed for the first time, which calls for detailed analysis and further experimental study to reveal device physics among key contribution factors.

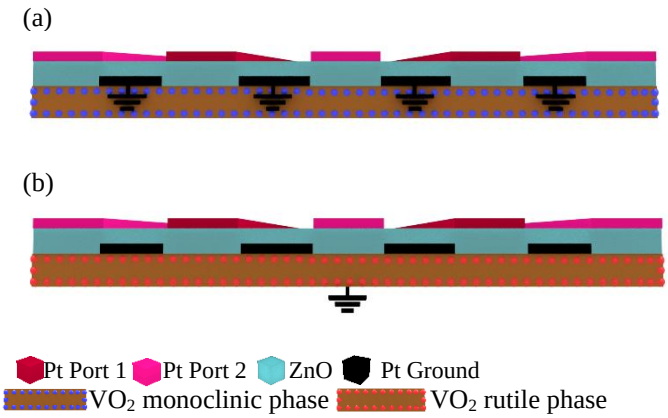


Fig. 2. Cross-section view of the two-port ZnO piezoelectric lateral extensional mode resonators with a thin-film $VO_2$ phase-transition material enabled reconfigurable bottom electrode, including both operation modes where (a) thin-film $VO_2$ is in the monoclinic (insulator) phase; (b) thin-film $VO_2$ in the rutile (metallic) phase

The device in this work is designed to operate in symmetrical width lateral-extensional modes. The resonance frequency of a $n^{th}$ order symmetrical width lateral-extensional mode resonator can be defined as (1):

$$f = \frac{n}{2W}\sqrt{\frac{E}{\rho}} \quad (1)$$

Where $n$ is the order of mode, $W$ is width of the resonator, $E$ is Young's modulus, and $\rho$ is density. The two-port top electrodes of the resonator in this work have a total of 5 IDT fingers, as shown in Fig. 2, which is designed for $5^{th}$ order (n=5) width lateral-extensional mode. The resonance mode at 86 MHz is the $3^{rd}$ order (n=3) lateral-extensional mode that is also detected by 5 IDT-finger top electrodes despite the slightly imperfect match between the modal strain field and the top electrode pattern.

The lower resonance frequency is the $3^{rd}$ order symmetrical width lateral-extensional mode, which is 86 MHz and 88 MHz based on FEM simulated and measured responses, respectively. This $3^{rd}$ order symmetrical width lateral-extensional mode only appears, when the $VO_2$ film is in its rutile (metallic) phase. The other resonance frequency is for the $5^{th}$ order symmetrical width lateral-extensional mode that is 152 MHz and 148 MHz based on FEM-simulated and measured responses, respectively. This $5^{th}$ order symmetrical width lateral-extensional mode appears when the $VO_2$ film is in either monoclinic (insulator) or rutile (metallic) phase. The slight discrepancy in resonance frequency from FEM simulation and measurement can be attributed to the difference in material properties, resonator's lateral dimensions (fabrication tolerance) and layer thicknesses used for simulation as compared to those of microfabricated and measured device.

## III. Finite Element Analysis of Piezoelectrically-Transduced Lateral Extensional Mode Resonators Equipped with a Reconfigurable Bottom Electrode

Finite element method (FEM) simulations have been used to model electrical and acoustic responses of the two-port ZnO piezoelectrically-transduced resonator with an embedded thin-film $VO_2$ phase-transition film that is underneath the ZnO piezoelectric transducer layer and slot-divided rectangular Pt bottom electrode. Fig. 3 presents the simulated broadband frequency characteristics using a three-dimensional (3D) FEM model of a two-port 320μm × 80μm rectangular-plate ZnO piezoelectric resonator equipped with a reconfigurable bottom electrode that can change back and forth between slotted and solid rectangular shape as shown in Fig. 2. The thin-film $VO_2$ can reversibly transform between its monoclinic (insulator) and rutile (metallic) phases with orders of magnitude change in conductivity. By transitioning into rutile phase when the temperature rises above 68°C, the conductive $VO_2$ layer completely fills and interconnects the divided slots of the Pt electrode to form a solid rectangular-shaped bottom electrode. Hence, the electric field distributions created between the two top IDT electrodes and reconfigurable bottom electrode vary drastically at the corresponding modal frequencies to result in unpresented mode switching behavior, which is a new design strategy that has never been reported.

Fig. 3 shows simulated frequency characteristics of the two lateral extensional mode resonances at frequencies of 86 MHz for $3^{rd}$ order symmetrical width lateral-extensional mode and 152MHz for $5^{th}$ order width symmetrical lateral-extensional mode, which are concurrently investigated in this work. There is a mode-switching behavior for the lateral extensional mode resonance at 86 MHz due to geometrical change of the bottom electrode between slot-divided and solid plate induced by the $VO_2$ film conductivity change during its phase transition. When the thin-film $VO_2$ is under its monoclinic (insulator) phase to retain the bottom electrode in its originally designed slot-divided rectangular shape (Fig. 2(a)), there is no resonance signal due to the lack of vertical electric field that can create an in-plane lateral modal vibration via transverse $d_{31}$ piezoelectric

coefficient to match the desired strain field needed for the targeted modal vibrations at 86 MHz. Meanwhile, when the thin-film $VO_2$ is under its rutile (metallic) phase (Fig 2(b)), the bottom electrode is composed of the slot-divided Pt electrode and conductive $VO_2$ film as a solid rectangular plate bottom electrode to create an enhanced vertical electric field that can induce a lateral modal vibration via transverse $d_{31}$ piezoelectric coefficient to match well with the desired strain field pattern for the corresponding lateral-extensional mode at 86 MHz.

As opposed to the aforementioned mode-switching behavior, the resonance at 152MHz shows a drastically different response, where both the signal level and the capacitive feedthrough level are elevated by roughly 15 dB when the $VO_2$ thin film underneath the Pt slot-divided bottom electrode transitions into its rutile (metallic) phase. Also, the resonance frequency shifts slightly due to the variation of the electric field patterns before and after electrode reconfiguration, which in turn changes the key characteristic dimension.

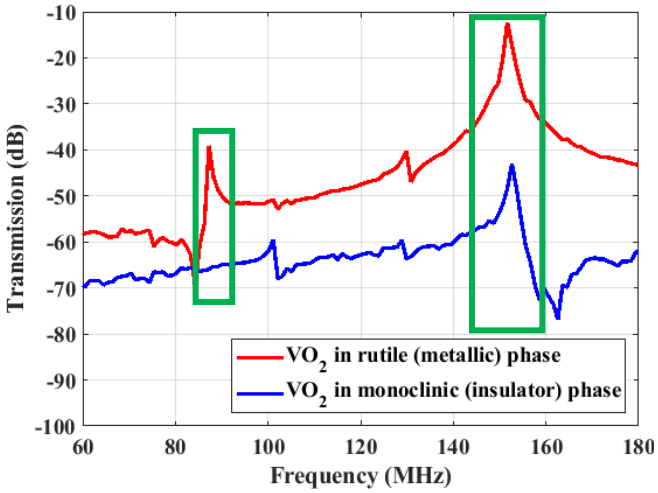


Fig. 3. The frequency response of two-port ZnO MEMS resonator with a reconfigurable bottom electrode growing on thin-film $VO_2$ by finite element analysis. The conductivity of the thin-film $VO_2$ in monoclinic or rutile phase impacts the resonance frequency and capacitive feedthrough level.

Fig. 4 presents the electric fields in two-dimension (2D) cross sectional view and the corresponding piezoelectrically-induced stress patterns in three-dimension (3D) schematic view by the reconfigurable bottom electrode, which is enabled by the phase transition of the thin-film $VO_2$. As seen by the FEM simulation, the electric field, displacement, and stress are confined between the interdigitated top electrodes and the reconfigurable bottom electrode. Due to two targeted resonance frequencies are 3rd and 5th order symmetric width lateral-extensional mode, the distribution and direction of the vertical electric field strength in the ZnO piezoelectric transducer layer and the transverse $d_{31}$ piezoelectric constant determine the strength of the resonance signal of desired resonance mode shape. Thus, the conductivity of thin-film $VO_2$ during phase transition impacts the bottom electrode geometry and the electric field, modal vibration, and frequency response are also impacted.

Fig. 4 (a) and (b) compare the electric field and stress patterns of a ZnO rectangular-plate, 3rd order symmetrical width lateral-extensional mode resonator operating at 86 MHz, which are generated by the reconfigurable bottom electrode enabled by the $VO_2$ thin film in its monoclinic and rutile phase, respectively. As shown, the orientation of the electric field underneath the three central top electrodes is flipped due to the electric field pattern in the ZnO layer is impacted by the slot-divided bottom electrode and the phase transition $VO_2$ thin film. The abrupt conductivity changes of the thin-film $VO_2$ during its phase transition from monoclinic to rutile phase to change the bottom electrode shape from slot divided plate to a solid rectangular plate. Moreover, the stress generated within the ZnO resonator body under the rutile phase of the thin-film $VO_2$ is noticeably stronger than the monoclinic phase. The vertical electric field strength and distribution, the transverse $d_{31}$ piezoelectric coefficient and the piezoelectrically-transduced strain pattern inside the ZnO piezo-transducer layer determines the resonance frequency strength. Thus, the FEM simulated modal resonance responses exhibit a mode-switching behavior for the 86 MHz 3rd order symmetrical width lateral-extensional mode as evidenced by the electric field and the stress patterns.

Meanwhile, Fig. 4 (c) and (d) depict the electric field and stress distributions that are induced by a reconfigurable bottom electrode of a ZnO rectangular-plate 5th order symmetrical width lateral-extensional mode resonator operating at 152 MHz by leveraging the $VO_2$ thin film in its monoclinic and rutile phase, respectively. As opposed to the resonance mode at 86 MHz, the directions of the electric fields and strain patterns stay largely unchanged before and after phase transition of thin-film $VO_2$ between monoclinic and rutile phases for reconfiguring the bottom electrode. As a result, the signal strength and capacitive feedthrough level of the 152 MHz resonance mode varies significantly, while the resonance frequency remains at 152 MHz before and after electrode reconfiguration to exhibit a dissimilar behavior apart from mode switching. The anti-resonance frequency at 158 MHz can be clearly observed when $VO_2$ film is under monoclinic (insulator) phase. Meanwhile, there is no significant anti-resonance frequency when $VO_2$ film is under rutile (metallic) phase due to the effect of elevated capacitive feedthrough level impacted by the bottom electrode geometrical change during the $VO_2$ phase transition. The dielectric loss in the resonator is also enhanced as temperature gradually increases. Thus, there is no detectable anti-resonance frequency, when $VO_2$ film is under rutile (metallic) phase.

(a)

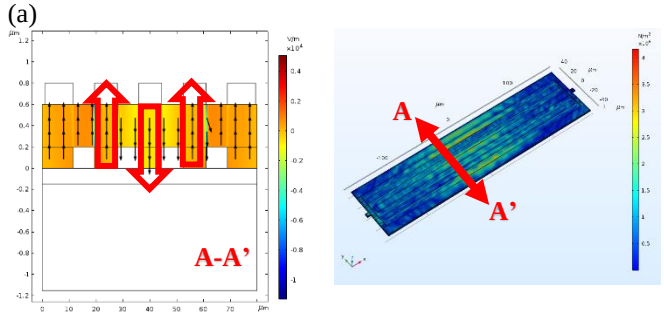

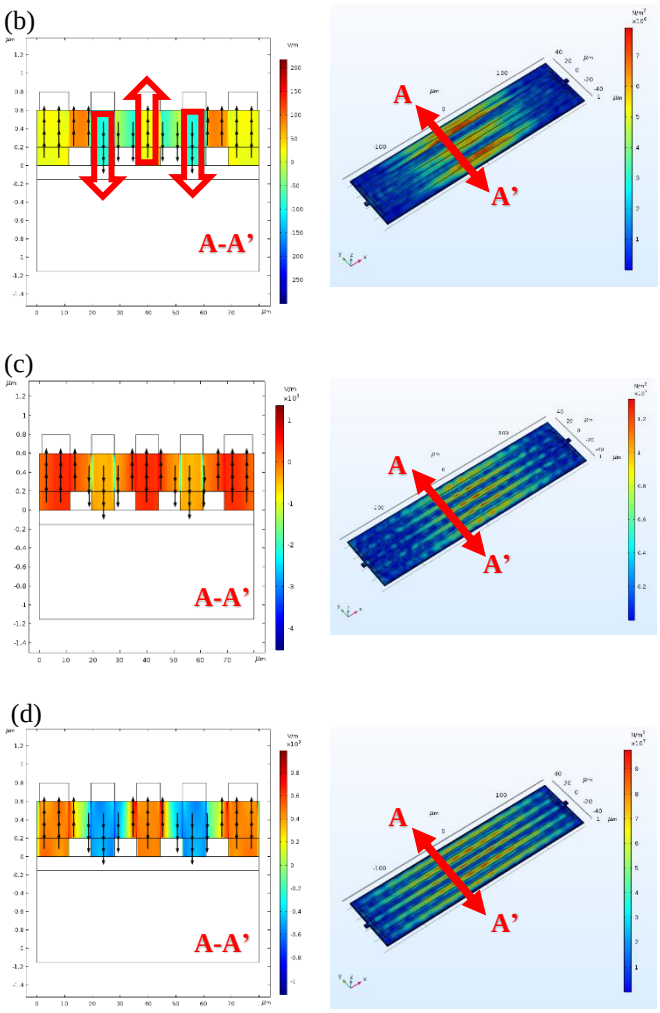


Fig. 4. Finite element analysis results that illustrate electric field change in two-dimensional (2D) and stress in three-dimensional (3D) diagrams due to the abrupt $VO_2$ conductivity change behavior during phase transition for two different resonance modes, including (a) electric field and stress patterns when $VO_2$ is under its monoclinic phase for the 86 MHz resonance; (b) electric field and stress patterns when $VO_2$ is under its rutile phase for the 86 MHz resonance; (c) electric field and stress patterns when $VO_2$ is under its monoclinic phase for the 152 MHz resonance; (d) electric field and stress patterns when $VO_2$ is under its rutile phase for the 152 MHz resonance.

## IV. Fabrication Process

The ZnO piezoelectric rectangular-plate, lateral-extensional mode resonators investigated in this work have been fabricated using the cleanroom facility at Nanotechnology Research and Education Center (NREC) of the University of South Florida, while the $VO_2$ thin films were deposited using pulsed laser deposition (PLD) by the Applied Material Group at the Michigan State University. Fig. 5 illustrates the step-by-step microfabrication process flow starting from a high-resistivity silicon wafer coated with a 1 µm-thick thermal oxide, which is followed by a blanket PLD deposition of a 150 nm-thick $VO_2$ layer right before deposition and patterning of the platinum (Pt) bottom electrode with a thickness of 200 nm by a lift-off step. The patterned Pt electrode and blanket $VO_2$ layer act as the bottom electrode of the ZnO piezoelectric transducer. Thereafter, a 550 nm-thick ZnO piezoelectric transducer layer is deposited by RF sputtering, followed by wet etching of ZnO to create via hole connecting the top and bottom electrodes. The platinum (Pt) top electrodes are deposited and patterned through a lift-off process. Then, a 10 µm-thick AZ-12XT photoresist is patterned as the dry-etching hard mask to define the resonator body. Similar to our prior works [13][42], a dry etch/releasing process that employs an inductively coupled plasma (ICP) etcher is conducted, which begins with reactive ion etching (RIE) of ZnO by $CH_4$ and Ar reactants, followed by $VO_2$ RIE etching by $SF_6$ and Ar reactants [43]. Subsequently, the $SiO_2$ layer is dry etched by $C_4F_8$, $CH_4$, and He gas reactants. Then, the dry releasing process starts with an anisotropic Si etching by a deep reactive ion etching process followed by isotropic dry etching of silicon underneath to fully suspend the resonator.

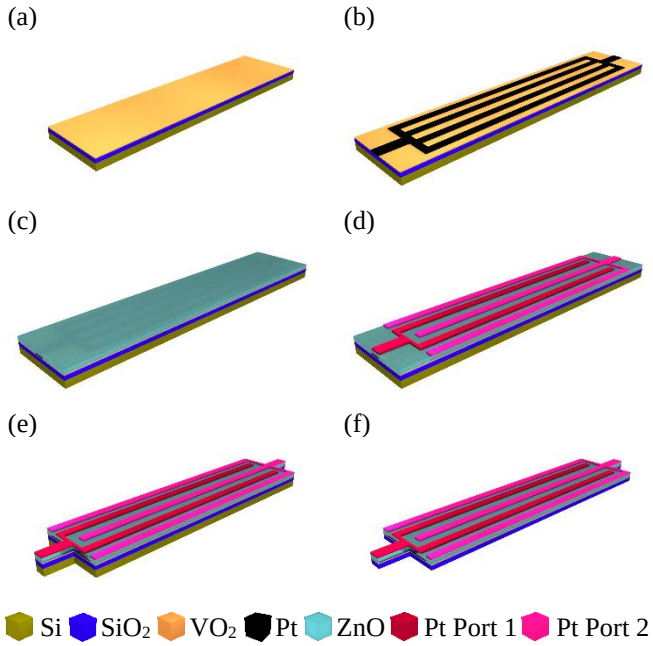


Fig. 5. Step-by-step fabrication process flow of ZnO lateral extensional mode resonators that are equipped with a reconfigurable bottom electrode enabled by the phase transition of the $VO_2$ thin film.

## V. Experiment Results

The microfabricated devices were measured using a Cascade 12000 RF probe station with a pair of 150 µm pitch ground-signal-ground (GSG) probes from GGB Industries Inc. The two-port scattering parameters (S-parameters) were measured by a Keysight Technology E5071C vector network analyzer, after an open-short-load-thru (OSLT) calibration using a CS-5 calibration standard substrate from GGB Industries Inc. The device temperature was controlled by a built-in thermal chuck during on-wafer probing, and the temperature was measured with a thermocouple along with a U5855A infrared camera from Keysight Technology.

Fig. 6 (a) shows a top-view microscope image of a fabricated two-port 320 µm × 80 µm rectangular-plate lateral extensional mode resonator that is equipped with five IDT fingers, two side-supporting tethers, and a reconfigurable bottom electrode that

is enabled by the phase transition of $VO_2$. All the measurement results are obtained from devices of this exact resonator design configuration with an exception of the bottom electrode shape. The thin-film $VO_2$ is under monoclinic (insulator) phase and rutile (metallic) phase when operating at 20°C and 95°C, respectively. As shown in Fig. 6 (b), the capacitive feedthrough level of broadband frequency response at 95°C is 6-10 dB higher than that measured at 20°C due to the orders of magnitude higher conductivity of the thin-film $VO_2$ when it undergoes phase transition from monoclinic to rutile phase. Meanwhile, the insertion loss for the 148 MHz ($5^{th}$ order symmetrical width lateral-extensional mode) resonance is lowered from 43.5 dB to 32.7 dB that can be mainly ascribed to elevated vertical electric field strength that generate stronger lateral modal vibration and modal strain pattern via transverse $d_{31}$ piezoelectric coefficient when the $VO_2$ thin film of the reconfigurable bottom electrode is under its rutile (metallic) phase to form a solid rectangular plate. As opposed to signal strength enhancement of the 148 MHz resonance, there is a more drastic mode-switching behavior for the resonance at 88 MHz ($3^{rd}$ order symmetrical width lateral-extensional mode) as shown in Fig. 6. In particular, there is no resonance peak at 88MHz when the device operates at 20°C. The thin-film $VO_2$ is under monoclinic (insulator) phase to cause a mismatch of the bottom electrode pattern in slot divided shape against the target mode shape and lack of desired electric field pattern to excite this resonance mode via transverse $d_{31}$ piezoelectric coefficient. On the contrary, a strong resonance signal appears at 88 MHz when the thin-film $VO_2$ change to its rutile (metallic) phase, thus reshaping the bottom electrode as a solid rectangular plate to create stronger vertical electric field and in-plane modal strain patterns induced by transverse $d_{31}$ piezoelectric effect for exciting the device into its modal vibration at 88 MHz through ZnO piezoelectric transducer. To the best of our knowledge, this unprecedented mode-switching behavior enabled by $VO_2$ phase transition and bottom electrode reconfiguration of a ZnO piezoelectric lateral-extensional mode resonator has never been reported previously.

(a)

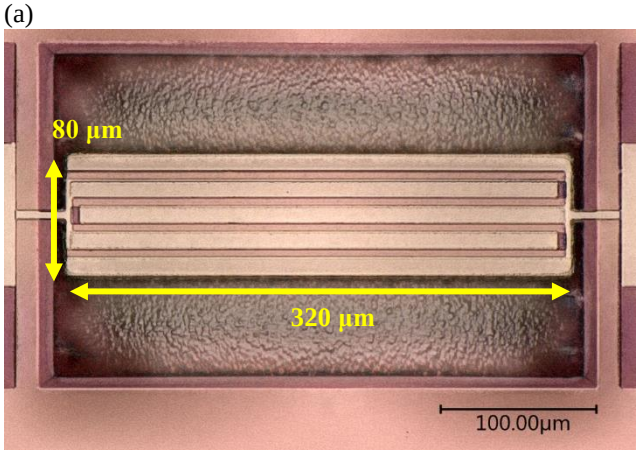


(b)

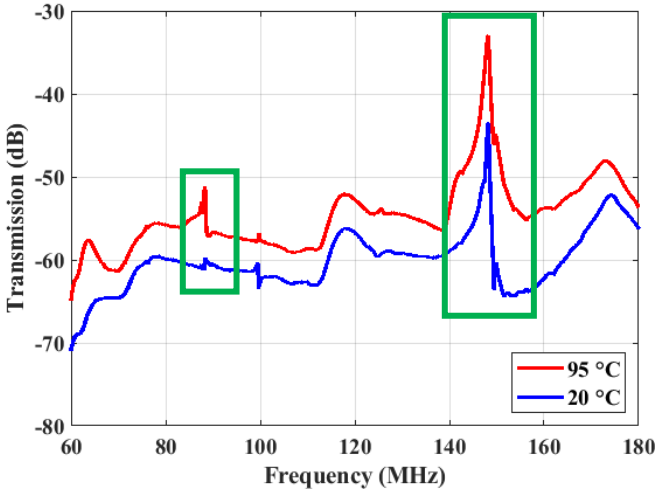


Fig. 6. (a) Top-view microscope image of a fabricated two-port 320 µm × 80 µm rectangular-plate lateral extensional mode resonator with five IDT fingers, two side-supporting tethers, and a reconfigurable bottom electrode that is enabled by the phase transition of $VO_2$ (b) Measured broadband frequency responses of a two-port MEMS resonator that is equipped with a reconfigurable bottom electrode composed of a $VO_2$ thin film that is embedded below the ZnO piezoelectric transducer layer and the Pt slot-divided rectangular-plate bottom electrode. Both the capacitive feedthrough and the resonance signal levels are elevated when the thin-film $VO_2$ is transitioned from its monoclinic (insulator) phase (20°C) to rutile (metallic) phase (95°C).

Fig. 7 (a) shows the frequency responses of a two-port ZnO MEMS resonator with embedded thin-film $VO_2$ underneath slot-divided rectangular-shaped Pt bottom electrode that have been characterized at temperatures between 20°C and 95°C with an increment of 20°C. As shown in Fig. 7 (a), the feedthrough and signal levels of the 148 MHz, which is $5^{th}$ order symmetrical width lateral-extensional mode, resonance gradually increase along with the temperature increase between 20°C and 60°C, whereas the largest boost of the resonance signal is observed when the thin-film $VO_2$ completes its phase transition during heating before reaching 95°C. At 95°C, the $VO_2$ film is under its rutile (metallic) phase thus converting the slotted bottom electrode into a solid rectangular plate, which results in much better aligned vertical electric field, $d_{31}$ piezoelectric constant and piezoelectrically-transduced strain patterns to exhibit a better spatial match with the target $5^{th}$ order symmetrical width lateral-extensional mode shape at 148 MHz.

Fig. 7 (b) shows frequency responses of a two-port MEMS rectangular-plate, $5^{th}$ order symmetrical width lateral-extensional mode resonator with $VO_2$ film embedded under a Pt solid rectangle plate bottom electrode, which are measured at temperatures between 20 and 95°C with an increment of 20°C. For this design, the phase-transition of thin-film $VO_2$ does not significantly impact the feedthrough and resonance signal levels, because the overlapping solid rectangular plate (slotted-less) electrode made of stacked $VO_2$ and Pt layers is dominated by the high conductivity of Pt bottom electrode instead of the effects of the $VO_2$ phase transition.

Fig. 7 (c) shows the $5^{th}$ order symmetrical width lateral-extensional mode frequency responses of a ZnO only two-port MEMS resonator with the same interdigital top electrodes and

slot-divided rectangular plate bottom electrode identical to the design shown in Fig. 7 (a), which are tested at temperature ranging from 20 to 95°C with an increment of 20°C. As opposed to tested temperature-dependent frequency responses with an embedded $VO_2$ phase-transition layer underneath the bottom electrode as shown in Fig. 7 (a), the measured frequency characteristics of the ZnO only resonators without $VO_2$ exhibit no noticeable change of both resonance signal and capacitive feedthrough levels, while exhibiting a linear temperature dependence of the resonance frequency. The measured resonance frequency decreases with rising temperature, showing a linear temperature dependence that can be largely attributed to the temperature dependence of Young's modulus of all structural materials and the lateral geometry expansion due to the temperature increase.

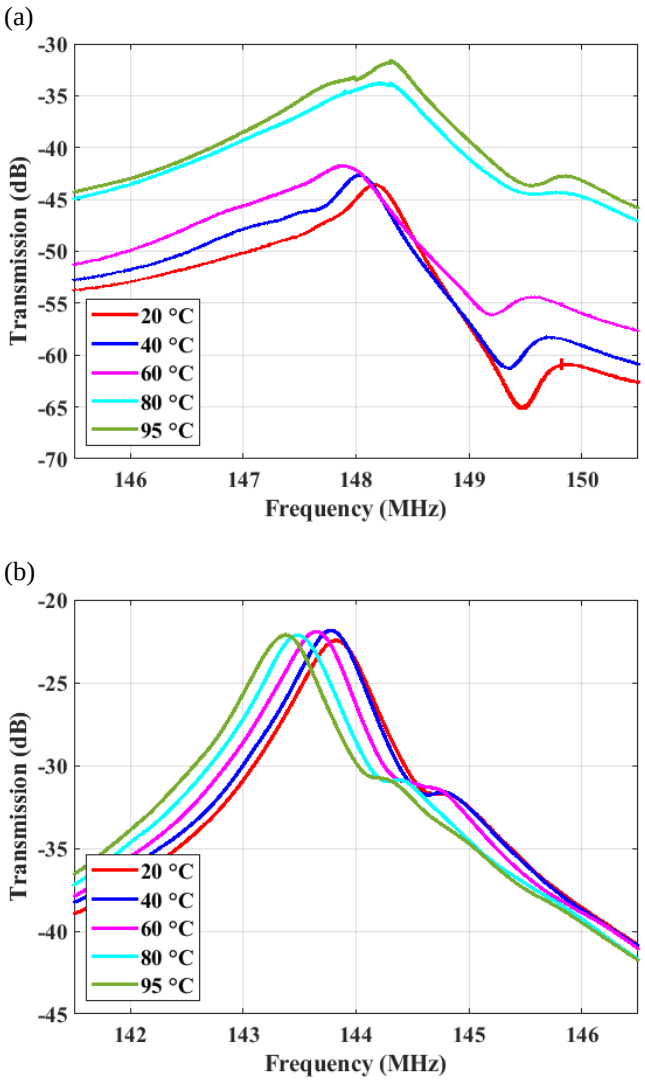


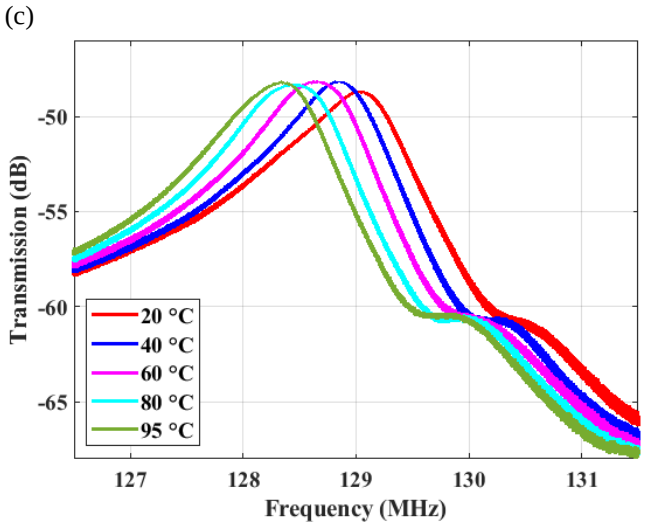


Fig. 7. The frequency responses of a two-port 5th order symmetrical width lateral-extensional mode ZnO only MEMS resonator measured during a heating cycle from 20 to 95°C with a 20°C increment, by showing the tested frequency characteristics of: (a) device with a slotted rectangular plate (reconfigurable) bottom electrode; (b) device with a solid rectangular plate (non-reconfigurable) bottom electrode; and (c) reference device with a Pt slotted rectangular plate bottom electrode but no $VO_2$ film.

Fig. 8 (a) and (b) show the frequency characteristics for the resonance mode at 88 MHz, 3rd order symmetrical width lateral-extensional mode of a two-port 320 μm × 80 μm rectangular-plate ZnO resonator with a reconfigurable bottom electrode composed of a $VO_2$ layer that are tested at temperature ranging from 20°C to 95°C during heating and cooling cycles with an increment of 20°C, respectively. Fig. 8 (c) and (d) show the hysteresis behavior of resonance frequency and insertion loss that are measured during heating and cooling cycles for the full temperature range between 60 to 95°C, respectively. As shown in Fig. 8 (a) and (b), the capacitive feedthrough level rises by 4-5 dB due to the thin-film $VO_2$ phase transition. To the best of our knowledge, this unique mode-switching behavior of a ZnO piezoelectric resonator by taking advantage of the electric field modification by a phase transition material has never been reported. Fig. 8 (c) shows the mode switch-on behavior of the 88 MHz resonance that starts at 70°C when the device is tested during a heating cycle, whereas the switch-off transition begins at 60°C during the cooling cycle. There is no resonance mode at 88MHz that can be observed below 70°C when a device is tested under a heating cycle. Similarly, there is no resonance mode below 60°C when a device is tested under a cooling cycle. The resonance frequency increases from 88.17 to 88.43 MHz when the temperature gradually ramps up from 70 to 95°C, while the resonance frequency decreases from 88.41 to 88.1 MHz when the device is cooling down from 95 to 60°C. Meanwhile, Fig. 8 (d) depicts the thermal hysteresis behavior in terms of the insertion loss for the 88 MHz resonance. When the device undergoes a gradual temperature increase from 70 to 95°C, the insertion loss lowers from 55.5 to 49.4 dB, whereas the insertion loss increases from 49.5 to 56.5dB while the device is cooling down from 95 to 60°C. The insertion loss is heavily dependent on vertical electric field strength to generate an in-plane lateral modal vibration/strain pattern via transverse $d_{31}$ piezoelectric effect to excite the 88MHz resonance mode.

These hysteresis behaviors indicate a different critical phase-transition temperature for the $VO_2$ between the heating and cooling cycles, where a higher phase transition temperature of 8-10°C has been observed during the heating cycle as compared to that of cooling cycle.

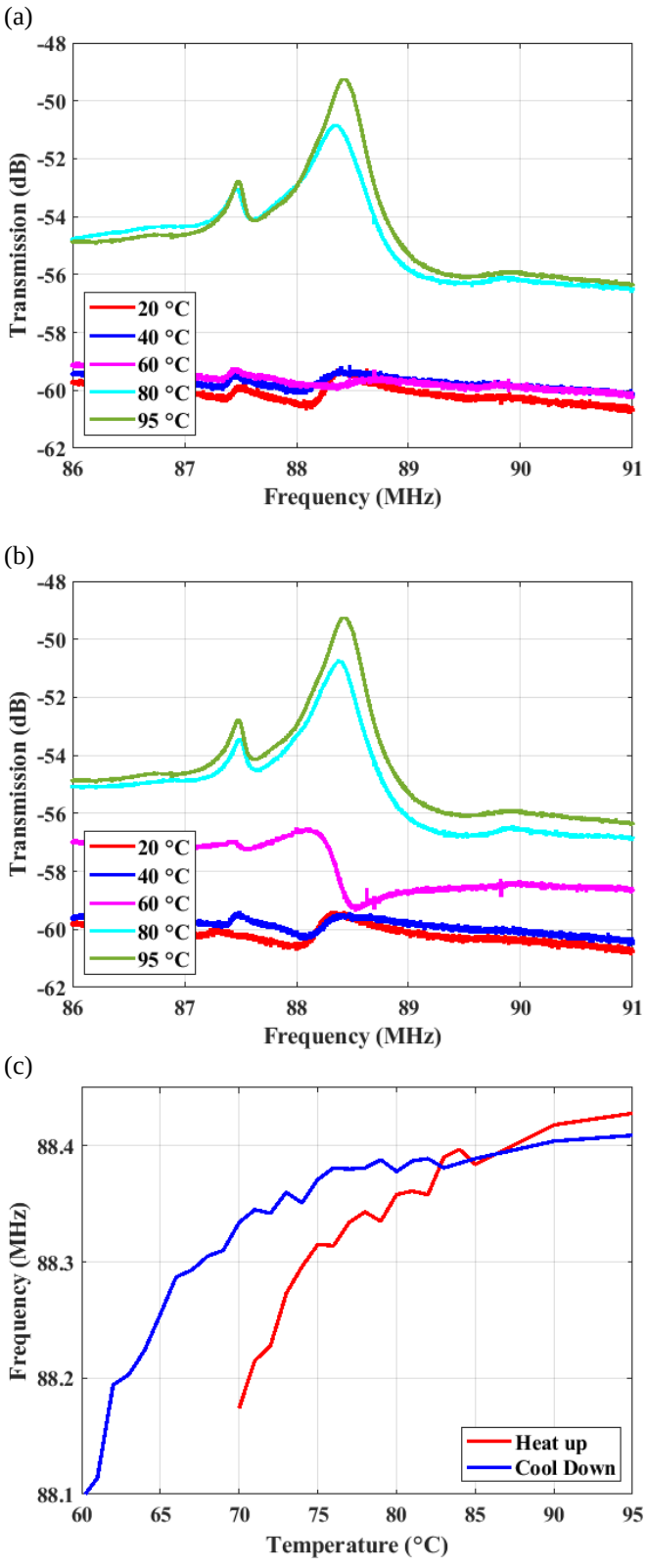


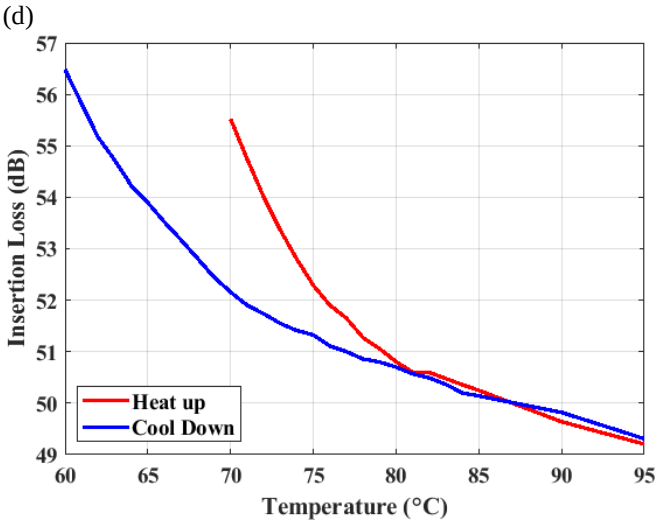


Fig. 8. Measured frequency responses of a two-port ZnO MEMS resonator with a reconfigurable bottom electrode that is composed of a $VO_2$ thin film underneath the ZnO piezoelectric transducer layer and Pt slotted rectangular plate bottom electrode for the 88 MHz resonance by showing the broadband frequency characteristics measured during (a) a heating cycle at temperature between 20°C and 95°C with a temperature increment of 20°C, (b) a cooling cycle at temperature between 20°C and 95°C with a temperature increment of 20°C. The thermal hysteresis loops across the temperature range of 60-95°C are also shown for both (c) resonance frequency, and (d) insertion loss.

Fig. 9 (a) and (b) show the measured frequency responses for the resonance mode at 148 MHz of the two-port rectangular-plate, 5th order symmetrical width lateral-extensional mode resonator with a reconfigurable bottom electrode composed of a $VO_2$ layer that are measured at temperature between 20°C and 95°C during heating and cooling cycles with an increment of 20°C, respectively. Fig. 9 (c) and (d) show the hysteresis behavior of resonance frequency and insertion loss that are measured during heating and cooling cycles for the temperature range between 20°C and 95°C, respectively. As shown in Fig. 9 (a) and (b), the capacitive feedthrough and resonance signal levels both increase during the phase transition of the $VO_2$ thin film from its monoclinic to rutile phase that transforms the shape of the bottom electrode to strengthen the electric fields and spatially match the desired mode shape, thus exciting the 148MHz lateral extension mode. Fig. 9 (c) and (d) show the measured thermal hysteresis loops of resonance frequency and insertion loss for heating and cooling cycles of the 148 MHz resonance for the temperatures between 20°C and 95°C. As shown in Fig. 9 (c), the resonance frequency increases from 148.16 MHz to 147.88 MHz, when the device undergoes a gradual temperature increase from 20°C to 60°C, which can be ascribed to temperature dependence of Young's modulus of all the constituent structural materials as the primary effect below the $VO_2$ transition temperature. The resonance frequency begins to shift higher from 147.88 to 148.3 MHz at a temperature between 60°C and 95°C, because the $VO_2$ layer's phase transition fully transforms the shape of the bottom electrode and the electric field pattern for modal excitation of piezoelectric resonator with a changed characteristic modal dimension. As evidenced by the FEM simulation and equivalent circuit model, electrode reconfiguration plays a major role in determining the temperature coefficient of resonance frequency at temperatures above $VO_2$ phase transition. Meanwhile, the

resonance frequency shift during temperature cycling also depends on the nonlinear variation of the Young's modulus of the $VO_2$ thin film due to the temperature change during phase transition [44] and conductivity variation of the slot-divided rectangular-plate (reconfigurable) bottom electrode that gradually increases due to the $VO_2$ thin film phase transition from monoclinic insulator phase and rutile (metallic) phase. Similarly, the resonance frequency of this lateral extension mode shifts lower from 148.3 to 147.94 MHz during the gradual phase transition of the thin-film $VO_2$ from rutile to monoclinic phase, while the device is cooling down from 95 to 50°C. Then, the resonance frequency rises from 147.94 to 148.15 MHz to exhibit a reverse temperature dependence, when it continues to cool down from 50 to 20°C. As seen in Fig. 9 (d), the insertion loss lowers from 43.5 dB to 31.5 dB during the heating cycle from 20 to 95°C, whereas the insertion loss increases from 31.6 to 43.5 dB during the cooling down from 95 to 20°C. The hysteresis loops of resonance frequency and insertion loss both indicate a 5-10°C discrepancy between the critical phase transition temperatures of the cooling and heating cycles.

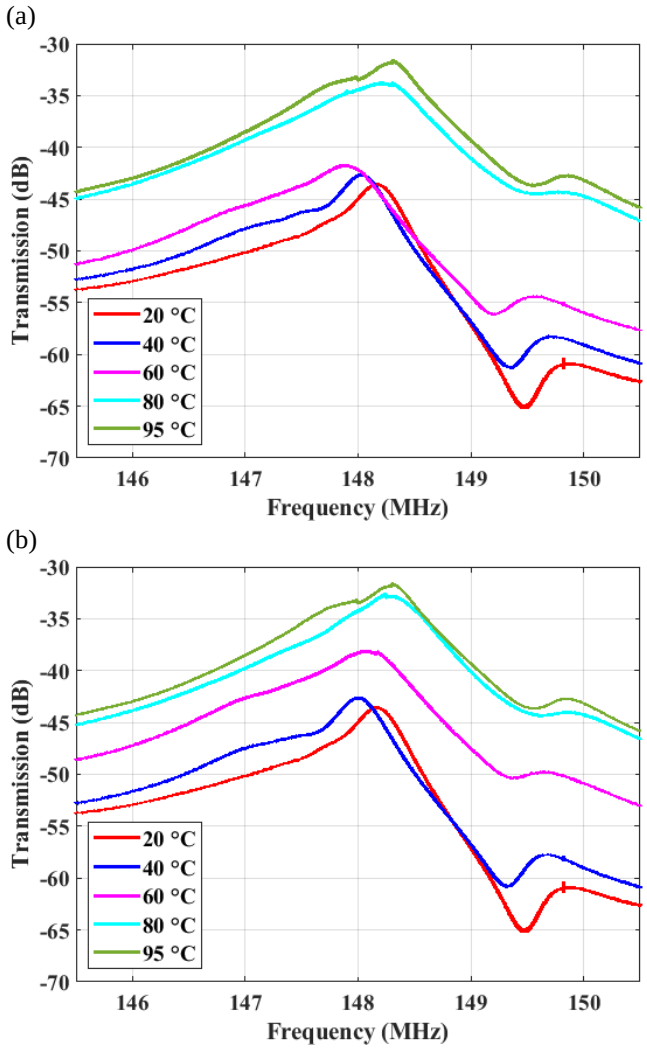


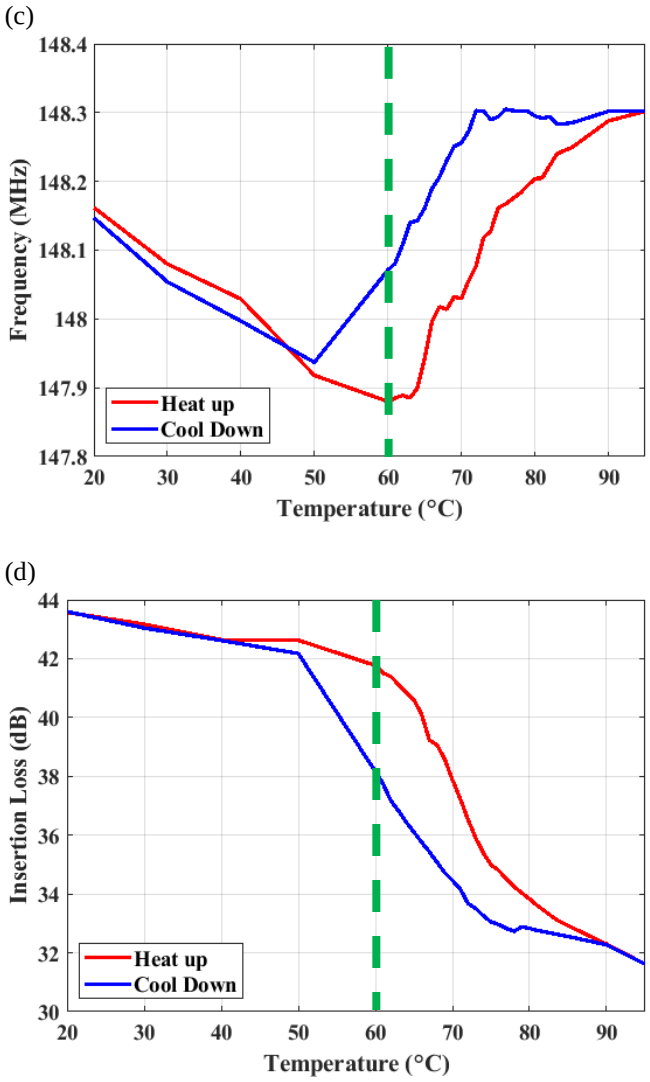


Fig. 9. The frequency responses of the two-port ZnO MEMS resonator with a reconfigurable bottom electrode composed of a $VO_2$ thin film underneath the ZnO piezoelectric transducer layer and slotted rectangular plate Pt bottom electrode for the 148 MHz resonance by showing the broadband frequency characteristics measured during (a) a heating cycle at temperature between 20 and 95°C with a temperature increment of 20°C, (b) a cooling cycle at temperature between 20 and 95°C with a temperature increment of 20°C. The thermal hysteresis loops across the temperature range of 20-95°C are also shown for both (c) resonance frequency, and (c) insertion loss.

## VI. Discussion

Fig. 10 presents a conceptual illustration diagram and the corresponding equivalent circuit model for the two-port piezoelectric resonator, where the $VO_2$ film underneath the piezoelectric transducer layer and the slot-divided rectangular Pt bottom electrode is under monoclinic and rutile phase, respectively. As depicted in Fig. 10, the full equivalent circuit model with varied static capacitance ($C_0$) induced by the reconfigurable bottom electrode is employed to analyze modal resonances at 148 MHz (5$^{th}$ order symmetrical width lateral-extensional mode) as example at 20°C and 95°C, which the $VO_2$ films are in monoclinic and rutile phase, respectively.

This article has been accepted for publication in a future issue of this journal, but has not been fully edited. Content may change prior to final publication. Citation information: DOI 10.1109/TUFFC.2022.3156845, IEEE Transactions on Ultrasonics, Ferroelectrics, and Frequency Control



Fig. 10 (a) shows the simulated and measured frequency responses based on measurement and equivalent circuit for the device at 20°C ($VO_2$ in monoclinic phase), while operating at 5th order lateral width extensional mode. Fig. 10 (b) shows the frequency responses based on measurement and equivalent circuit model for the device at 95°C ($VO_2$ in rutile phase), while operating at 5th lateral width-extensional mode. There is a spurious mode at ~149 MHz adjacent to 5th lateral-extensional mode at 148 MHz. In order to model these two resonances of similar resonance frequencies, two shunt RLC equivalent circuits are employed to capture their resonance responses. The $R_m$, $L_m$ and $C_m$ are used to simulate the 5th order lateral-extensional mode and $R'_m$, $L'_m$ and $C'_m$ are included to simulate the frequency response of that spurious mode. The cross-field capacitance ($C_0$) when device is operating at 20°C under its monoclinic phase is created by $C_{Pt}$, which is the capacitance between IDT top electrodes and slot-divided bottom electrode. $C_{Pt}$, is 9.3 fF in the equivalent circuit model. The values for $R_m$, $L_m$ and $C_m$ for 5th order symmetrical lateral width-extensional mode and the $R'_m$, $L'_m$ and $C'_m$ at 95°C for the spurious mode are listed in Table 1 below. When the resonator is heated up to 95°C, the $VO_2$ film changes its phase from monoclinic (isolator) phase to rutile (metallic) phase. Due to the $VO_2$'s phase transition to become conductive, the bottom electrode shape is converted to a solid rectangular plate from the originally designed slot-divided rectangular electrode. The cross-field capacitance ($C_0$) at 95°C include both $C_{Pt}$ and $C_{VO2}$, which is capacitance between conductive $VO_2$ film and top electrodes. $C_{VO2}$ is determined to be 10.5 fF that is comparably higher than 9.3 fF when $VO_2$ is under monoclinic phase largely due to enlarged bottom electrode from slot divided to solid rectangular plate during $VO_2$'s phase transition. And the $C_{VO2}$ is parallel to the $C_{Pt}$. Thus, the cross-field capacitance ($C_0$) when device at 95°C is ascribed to a combined effect of both $C_{Pt}$ and $C_{VO2}$, which is 19.8 fF. The values for $R_m$, $L_m$ and $C_m$ for 5th order symmetrical lateral-extensional mode and the $R'_m$, $L'_m$ and $C'_m$ at 95°C for spurious mode are shown in Table 1 below.

Table 1. The parameters of the equivalent circuit model extracted from the measurement data when the device at 20°C and 95°C

| | Cross-field capacitance ($C_0$) | | 5th order symmetrical lateral width extensional mode | | | Spurious mode | | |
|---|---|---|---|---|---|---|---|---|
| Temp. (°C) | $C_{Pt}$ (fF) | $C_{VO2}$ (fF) | $R_m$ (Ω) | $L_m$ (μH) | $C_m$ (fF) | $R'_m$ (Ω) | $L'_m$ (μH) | $C'_m$ (fF) |
| 20 | 9.3 | - | 3,900.5 | 1,050.0 | 1.1 | 3,600.5 | 898.0 | 1.3 |
| 95 | 9.3 | 10.5 | 1,310.5 | 281.1 | 4.1 | 440.5 | 100.4 | 11.3 |

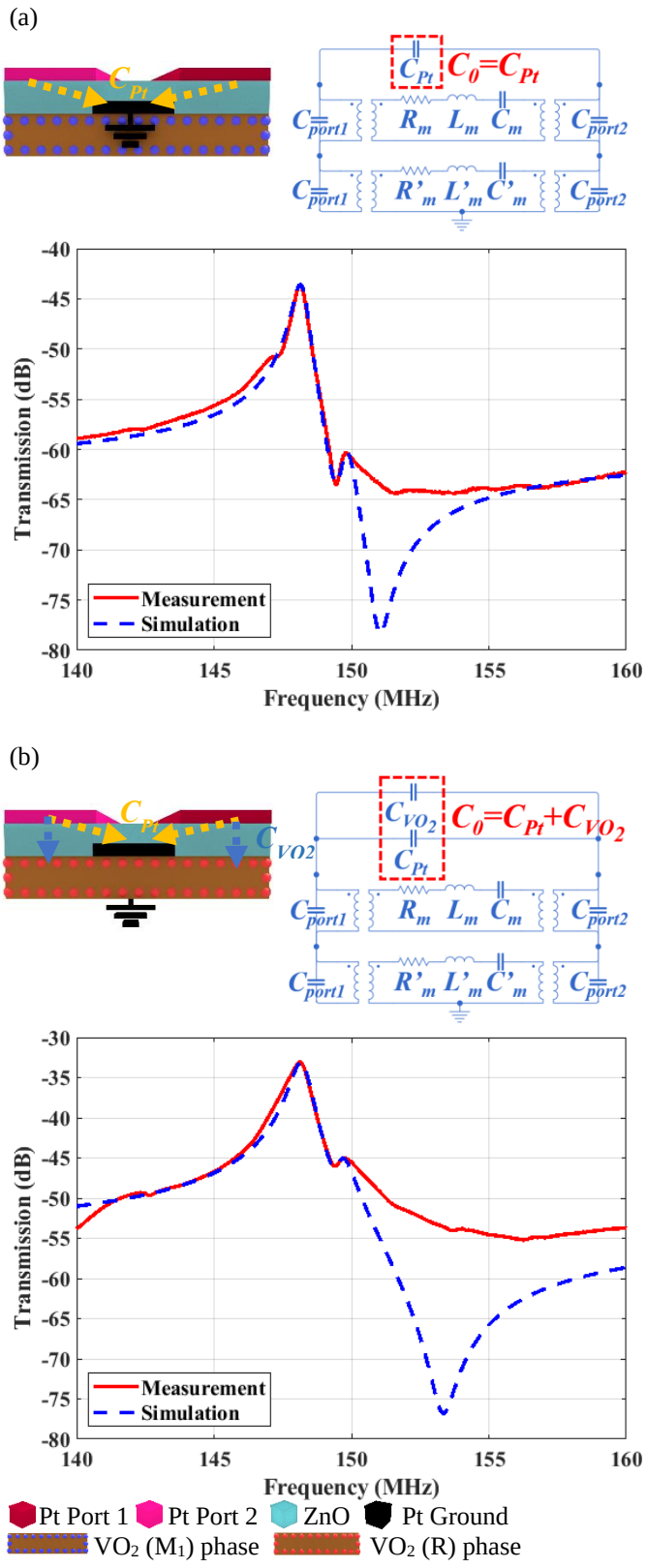


Fig. 10. A conceptual illustration diagram for modeling the capacitive feedthrough level in a two-port 5th order symmetrical width lateral-extensional mode piezoelectric resonator and equivalent static capacitance ($C_0$) in a corresponding equivalent circuit model, where the $VO_2$ layer is under (a) monoclinic phase, and (b) rutile phase.

Fig. 11 (a) shows the temperature coefficient of frequency (TCF) of a two-port ZnO MEMS resonator with embedded thin-film $VO_2$ underneath a slot-divided, rectangular-plate Pt bottom electrode that are characterized at 5$^{th}$ order symmetrical width lateral-extensional mode at temperature between 20°C and 95°C with an increment of 10°C. As shown in Fig. 11 (a), the resonance frequency shows a linear dependence during both heating and cooling cycles when $VO_2$ film is under monoclinic insulator phase. The extracted TCF is -48.93 ppm/°C when the device undergoes a gradual temperature increase from 20°C to 60°C during a heating cycle, whereas a TCF of -46.35 ppm/°C is observed when it is cooling down from 50°C to 20°C.

Fig. 11 (b) presents the measured 5$^{th}$ order symmetrical width lateral-extensional mode resonance frequency over a temperature range between 20°C and 95°C with an increment of 10°C and the extracted TCF values of a two-port ZnO MEMS resonator with $VO_2$ thin-film embedded under a solid rectangle plate Pt bottom electrode. As shown in Fig. 11 (b), the TCF of this device is -45.22 ppm/°C when the device undergoes a gradual temperature increase from 20°C to 95°C during heating cycle, whereas a TCF of -46.98 ppm/°C is obtained when the device is gradually cooling down from 95°C to 20°C. Under heating and cooling cycles, the resonance frequency exhibits a linear dependence upon the temperature change for this design a solid rectangular-plate (slotted-less) bottom electrode made of stacked $VO_2$ and Pt layers. Consequently, the phase transition of the $VO_2$ layer that directly overlaps with a highly conductive Pt electrode makes little impacts on the bottom electrode shape. It is worthwhile mentioning that the rectangular plate resonator design with a solid rectangular plate Pt bottom electrode and an embedded $VO_2$ layer retains all design parameters identical to those of the slot-divided design. Obviously, these two resonator designs that are both equipped with an identical layer stack and geometrical parameters of the resonator body and top electrodes have exhibited very different temperature dependence of resonance frequency over the temperature range between 20 and 95°C. Therefore, the phase-transition dependent nonlinear TCF behavior can no longer be mainly ascribed to temperature dependence of the Young's modulus of all the stacked resonator structural layers including $VO_2$, the abrupt change of electrical field and piezoelectrically-induced stress patterns before and after the bottom electrode reconfiguration is anticipated to play a dominant role in leading to nonlinear temperature dependence especially at temperatures above the IMT transition of $VO_2$.

Fig. 11 (c) shows the TCF of a ZnO only MEMS resonator at 5$^{th}$ order symmetrical lateral-extensional mode with the same interdigital top electrodes and slotted rectangular plate bottom electrode identical to the design with embedded $VO_2$ as shown in Fig. 11 (a), which are measured at temperature ranging from 20 to 95°C with an increment of 10°C. To act as a reference device without a built-in $VO_2$ phase-transition layer underneath bottom electrode, the TCF of the ZnO only resonators without the $VO_2$ layer is -70.28 ppm/°C when the device undergoes a gradual temperature increase from 20 to 95°C, while a similar TCF of -64.70 ppm/°C is observed when the device is gradually cooling down from 95 to 20°C. The measured TCF in Fig. 11 (a) and (c) are quite different, which suggests the embedded $VO_2$ layer instead of the slot-divided bottom electrode design strongly impacts resonance frequency and its temperature dependence during the heating and cooling cycle. Meanwhile, Fig. 11 (a) and (b) shows similar linear TCF behaviors of comparable TCF values, as these two designs have different bottom electrode geometry and the resonator body layer stack constitution. As the $VO_2$ film embedded underneath the original Pt bottom electrode acts as an insulation layer under monoclinic phase and Pt has superior conductivity as compared to that of $VO_2$ under its rutile (metallic) phase, it is anticipated for the design with solid rectangular plate Pt bottom electrode to exhibit no noticeable change in its frequency response such as mode switching or resonance signal level boosting, when it undergoes a temperature variation between 20 and 95°C. On the contrary, the effects of thin-film $VO_2$ phase transition on the resonance signal characteristics are clearly observed in design with slot-divided bottom electrode that enables reconfiguration of the bottom electrode in terms of its geometry as can be seen in Fig. 7, 8, 9, and 11. At the same time, the measured TCF is slightly lowered due to the incorporation of $VO_2$ layer that is evidenced when comparing results shown in Fig. 11 (b) and (c), which can be attributed to the Young's modulus temperature dependence of the $VO_2$ thin film similar to prior works [44]. As shown in Fig. 11(a), the $VO_2$ thin film starts its phase transition from monoclinic (insulator) phase to rutile (metallic) phase after reaching 60°C during a heating cycle. The resonance frequency shifts from 147.88 to 148.3MHz, when the temperature rises from 60 and 95°C due to thin-film $VO_2$ phase transition, which completely transforms the shape of the bottom electrode and the electric field pattern for spatially matched mode excitation of the 148MHz lateral extensional mode and modification of the effective static capacitance represented by $C_0$ in the equivalent circuit model. The V-shape resonance frequency dependence upon the temperature is a combined effect of a changed characteristic dimension and total static capacitance due to the electrode reconfiguration, Young's modulus temperature dependence of the $VO_2$ thin film during its phase transition, and conductivity variation of the slot-divided rectangular-plate (reconfigurable) bottom electrode that gradually increases due to the $VO_2$ thin film phase transition from monoclinic (insulator) phase and rutile (metallic) phase. A great deal of resonator design and fabrication process change is required in order to isolate the contributions of the effects of the electrode or electric field reconfiguration and temperature dependence of the Young's modulus of the $VO_2$ thin film, which is beyond the scope of this work.

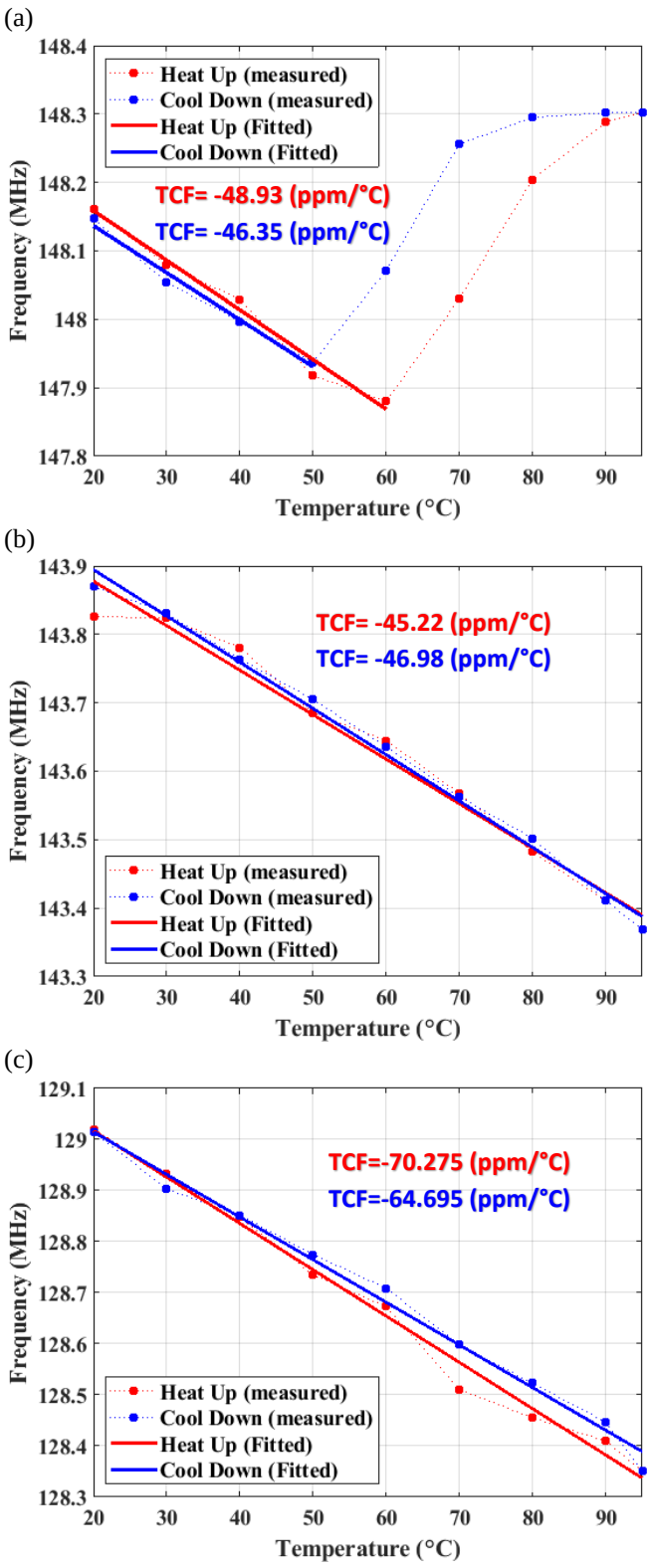


Fig. 11. The temperature coefficient of frequency (TCF) of the two-port ZnO MEMS resonator during a heating and cooling cycle from 20°C and 95°C with a 10°C increment, by showing the frequency characteristics of (a) a design with a slot-divided rectangular-plate (reconfigurable) bottom electrode, (b) a design with a solid rectangular plate (non-reconfigurable) bottom electrode, and (c) a ZnO only reference design with a slot-divided rectangular plate bottom electrode that is not equipped with a $VO_2$ thin film.

## VII. Conclusion

This paper presents a two-port rectangular-plate, lateral-extensional mode ZnO piezoelectric resonator with a reconfigurable bottom electrode by embedding a vanadium dioxide ($VO_2$) thin film as a phase transition material. As a result of the temperature variation, the phase transition of the $VO_2$ thin film buried underneath the slot-divided Pt electrode transforms the geometry of the bottom electrode, therefore dramatically varying the electric field distribution and piezoelectrically-transduced strain patterns. Consequently, a unique and unprecedented resonance mode-switch behavior enabled by $VO_2$ phase transition has been observed for the first time. FEM analysis was employed to model the broadband frequency responses and significant change of the electric field and strain field patterns before and after the reconfiguration of bottom electrode's geometry was observed. In order to characterize the temperature dependance, frequency responses of a two-port resonator have been measured over a temperature range between 20 and 95°C while focusing on two specific resonances at 88 and 148 MHz. Both the feedthrough and resonance signal levels have shown a strong dependence on the hysteretic behavior of $VO_2$ thin film during a heating or cooling cycle. The unique mode switch-on behavior of the 88 MHz resonance starts at 70°C during a heating cycle and switch-off transition begins at 60°C during a cooling cycle due to the abrupt electric field modification by reconfigurable bottom electrode. Moreover, a decrease of the insertion loss and resonance frequency of 12 dB and 0.28 MHz, respectively, have been observed for the 148 MHz resonance in response to a temperature increase from 20 to 60°C that is below the phase transition temperature. This suggests that the temperature dependence of Young's modulus of all constituent structural materials including $VO_2$ play a dominant role below the transition temperature. Meanwhile, a resonance frequency increase of 0.42 MHz was observed during a further temperature increase from 60 to 95°C that can be ascribed to combined effects of static capacitance increase due to bottom electrode reconfiguration, Young's modulus temperature dependence of $VO_2$ during its phase transition, and better piezoelectrically-transduced strain field to mode shape match when the bottom electrode is converted from a slot-divided plate into a solid rectangular plate geometry. The equivalent circuit model also confirms a capacitive feedthrough level increase and resonance frequency shift when $VO_2$ is transitioned from monoclinic (insulator) to rutile (metallic) phase. Three resonator designs with identical top IDT electrodes have been jointly investigated, including two devices with $VO_2$ embedded underneath a slot-divided rectangular plate and a solid rectangular plate bottom electrode, respectively, as well as one design with a slot-divided rectangular plate bottom electrode but no $VO_2$. As indicated by the measured temperature coefficient of resonance frequency (TCF), both the bottom electrode reconfiguration and $VO_2$ phase transition influence the resonance frequency responses that exhibit a nonlinear dependence upon the temperature variation across the temperature range between 60°C and 95°C.

## ACKNOWLEDGMENT

The authors would like to thank R. Everly, R. Tufts, Y. Emirov, and J. Bieber from the Nanotechnology Research and Education Center at University of South Florida for their technical supports and GGB Inc. for supplying all the RF probes and calibration substrates. In addition, we would also like to acknowledge the Florida High Tech Corridor program for providing partial financial support for this research.

## REFERENCES

[1] C. T.-C. Nguyen, "MEMS technology for timing and frequency control," IEEE Transactions on Ultrasonics, Ferroelectrics and Frequency Control, vol. 54, no. 2, pp. 251–270, 2007.

[2] Y. Xie, S.-S. Li, Y.-W. Lin, Z. Ren, and C. T.-C. Nguyen, "1.52-GHz micromechanical extensional wine-glass mode ring resonators," IEEE Transactions on Ultrasonics, Ferroelectrics and Frequency Control, vol. 55, no. 4, pp. 890–907, 2008.

[3] J. Wang, Z. Ren, and C. T.-C. Nguyen, "1.156-GHz self-aligned vibrating micromechanical disk resonator," IEEE Transactions on Ultrasonics, Ferroelectrics and Frequency Control, vol. 51, no. 12, pp. 1607–1628, 2004.

[4] J. Wang, J. E. Butler, T. Feygelson and C. T. -C. Nguyen, "1.51-GHz nanocrystalline diamond micromechanical disk resonator with material-mismatched isolating support," 17th IEEE International Conference on Micro Electro Mechanical Systems. Maastricht MEMS 2004 Technical Digest, pp. 641-644, 2004.

[5] R. Ruby and P. Merchant, "Micromachined thin film bulk acoustic resonators," Proceedings of IEEE 48th Annual Symposium on Frequency Control, 1994.

[6] G. G. Fattinger, J. Kaitila, R. Aigner, and W. Nessler, "Thin film bulk acoustic wave devices for applications at 5.2 GHz," IEEE Symposium on Ultrasonics, 2003.

[7] G. Piazza, P. J. Stephanou, and A. P. Pisano, "Piezoelectric Aluminum Nitride Vibrating Contour-Mode MEMS Resonators," *Journal of Microelectromechanical Systems*, vol. 15, no. 6, 2006.

[8] S. Gong, and G. Piazza, "Figure-of-Merit Enhancement for Laterally Vibrating Lithium Niobate MEMS Resonators" *IEEE Transactions on Electron Devices*, vol. 60, no. 11, pp. 3888-3894, 2013.

[9] S. Gong, and G. Piazza, "Design and Analysis of Lithium–Niobate-Based High Electromechanical Coupling RF-MEMS Resonators for Wideband Filtering" *IEEE Transactions on Microwave Theory and Techniques*, vol. 61, no. 1, pp. 403-414, 2013.

[10] Y. Yang, A. Gao, R. Lu, and S. Gong, "5 GHz Lithium Niobate MEMS Resonators with High FOM of 153," 2017 IEEE 30th International Conference on Micro Electro Mechanical Systems (MEMS), pp. 942-945, 2017.

[11] M. Link, M. Schreiter, J. Weber, R. Primig, D. Pitzer, and R. Gabl, "Solidly mounted ZnO shear mode film bulk acoustic resonators for sensing applications in liquids," IEEE Transactions on Ultrasonics, Ferroelectrics and Frequency Control, vol. 53, no. 2, pp. 492–496, 2006.

[12] G. K. Ho, R. Abdolvand, A. Sivapurapu, S. Humad, and F. Ayazi, "Piezoelectric-on-Silicon Lateral Bulk Acoustic Wave Micromechanical Resonators," *Journal of Microelectromechanical Systems*, vol. 17, no. 2, pp. 512–520, 2008.

[13] X. Han, D. Lan, and J. Wang, "ZnO-on-Diamond Resonators with Notched Thin-Film Piezoelectric Interdigital Transducer for Enhanced Signal-to-Noise Ratio and Feedthrough Suppression," *2020 IEEE 33rd International Conference on Micro Electro Mechanical Systems (MEMS)*, 2020.

[14] Q. -. Su, P. Kirby, E. Komuro, M. Imura, Q. Zhang and R. Whatmore, "Thin-film bulk acoustic resonators and filters using ZnO and lead-zirconium-titanate thin films," in *IEEE Transactions on Microwave Theory and Techniques*, vol. 49, no. 4, pp. 769-778, 2001.

[15] J. S. Pulskamp, R. Q. Rudy, S. S. Bedair, J. M. Puder, M. G. Breen and R. G. Polcawich, "Ferroelectric PZT MEMS HF/VHF resonators/filters," *2016 IEEE International Frequency Control Symposium (IFCS)*, pp. 1-4, 2016.

[16] H. Chandrahalim, S. A. Bhave, R. G. Polcawich, J. S. Pulskamp and R. Kaul, "PZT transduction of high-overtone contour- mode resonators," in *IEEE Transactions on Ultrasonics, Ferroelectrics, and Frequency Control*, vol. 57, no. 9, pp. 2035-2041, 2010.

[17] R. Abdolvand, B. Bahreyni, J. Lee, and F. Nabki, "Micromachined Resonators: A Review," *Micromachines*, vol. 7, no. 9, p. 160, 2016.

[18] O. Mortada, A. H. Zahr, J.-C. Orlianges, A. Crunteanu, M. Chatras, and P. Blondy, "Analysis and optimization of acoustic wave micro-resonators integrating piezoelectric zinc oxide layers," *Journal of Applied Physics*, vol. 121, no. 7, p. 074504, 2017.

[19] M. Rinaldi, C. Zuniga, C. Zuo, and G. Piazza, "Ultra-thin Super High Frequency two-port ALN contour-mode resonators and filters," *TRANSDUCERS 2009 - 2009 International Solid-State Sensors, Actuators and Microsystems Conference*, 2009.

[20] S. Yazici, M. Giovannini, N.-K. Kuo and G. Piazza, "Suppression of Spurious Modes via Dummy Electrodes and 2% Frequency Shift via Cavity Size Selection for 1 GHz AlN MEMS Contour-Mode Resonators," *2012 IEEE International Frequency Control Symposium Proceedings*, pp. 1-5, 2012.

[21] J. Segovia-Fernandez, M. Cremonesi, C. Cassella, A. Frangi and G. Piazza, "Anchor Losses in AlN Contour Mode Resonators," in *Journal of Microelectromechanical Systems*, vol. 24, no. 2, pp. 265-275, April 2015.

[22] A. Lozzi, L. G. Villanueva and E. T. Yen, "Anchor loss dependence on electrode materials in contour mode resonators," *2016 IEEE International Frequency Control Symposium (IFCS)*, pp. 1-4, 2016.

[23] J. Segovia-Fernandez, N. Kuo and G. Piazza, "Impact of metal electrodes on the figure of merit (kt2·Q) and spurious modes of contour mode AlN resonators," *2012 IEEE International Ultrasonics Symposium*, pp. 299-302, 2012.

[24] J. Zou and C. S. Lam, "Electrode design of AlN Lamb wave resonators," *2016 IEEE International Frequency Control Symposium (IFCS)*, pp. 1-5, 2016.

[25] C. Zuo, N. Sinha and G. Piazza, "Novel electrode configurations in dual-layer stacked and switchable ALN contour-mode resonators for low impedance filter termination and reduced insertion loss," *2010 IEEE 23rd International Conference on Micro Electro Mechanical Systems (MEMS)*, pp. 719-722, 2010.

[26] C. Cassella, J. Segovia-Fernandez and G. Piazza, "Segmented electrode excitation of aluminum nitride contour mode resonators to optimize the device figure of merit," *2013 Transducers & Eurosensors XXVII: The 17th International Conference on Solid-State Sensors, Actuators and Microsystems (TRANSDUCERS & EUROSENSORS XXVII)*, pp. 506-509, 2013.

[27] C.-M. Lin, V. Yantchev, Y.-Y. Chen, V. V. Felmetsger, and A. P. Pisano, "Characteristics of AlN Lamb wave resonators with various bottom electrode configurations," *2011 Joint Conference of the IEEE International Frequency Control and the European Frequency and Time Forum (FCS) Proceedings*, 2011.

[28] S. I. Jung, C. Ryu, G. Piazza, and H. J. Kim, "A Study on the Effects of Bottom Electrode Designs on Aluminum Nitride Contour-Mode Resonators," *Micromachines*, vol. 10, no. 11, p. 758, 2019.

[29] S. I. Jung, G. Piazza, and H. J. Kim, "The Impact of Bottom Electrode Coverage Rate on Electromechanical Coupling and Quality Factor of AlN MEMS Contour Mode Resonators," *2019 20th International Conference on Solid-State Sensors, Actuators and Microsystems & Eurosensors XXXIII (TRANSDUCERS & EUROSENSORS XXXIII)*, 2019.

[30] G. Hummel, Y. Hui and M. Rinaldi, "Reconfigurable Piezoelectric MEMS Resonator Using Phase Change Material Programmable Vias," in *Journal of Microelectromechanical Systems*, vol. 24, no. 6, pp. 2145-2151, 2015.

[31] Y. Shim, G. Hummel, and M. Rais-Zadeh, "RF switches using phase change materials," *2013 IEEE 26th International Conference on Micro Electro Mechanical Systems (MEMS)*, 2013.

[32] N. El-Hinnawy, P. Borodulin, E. Jones, B. Wagner, M. King, J. Mason, J. Hartman, R. Howell, M. Lee, and R. Young, "Improvements in GeTe-Based Inline Phase-Change Switch Technology for RF Switching Applications," *CS Mantech Conference*, 2014.

[33] G. Rebeiz, K. Entesari, I. Reines, S.-j. Park, M. El-tanani, A. Grichener, and A. Brown, "Tuning in to RF MEMS," *IEEE Microwave Magazine*, vol. 10, no. 6, pp. 55-72, 2009.

[34] [34] F. J. Morin, "Oxides Which Show a Metal-to-Insulator Transition at the Neel Temperature," *Physical Review Letters*, vol. 3, no. 1, pp. 34–36, 1959.

[35] A. Rúa, F. E. Fernández, and N. Sepúlveda, "Bending in VO2-coated microcantilevers suitable for thermally activated actuators," *Journal of Applied Physics*, vol. 107, no. 7, p. 074506, 2010.

[36] P. Jin, S. Nakao, S. Tanemura, T. Bell, L. S. Wielunski, and M. V. Swain, "Characterization of mechanical properties of VO2 thin films on sapphire and silicon by ultra-microindentation," *Thin Solid Films*, vol. 343-344, pp. 134–137, 1999.

[37] A. S. Barker, H. W. Verleur, and H. J. Guggenheim, "Infrared Optical Properties of Vanadium Dioxide Above and Below the Transition Temperature," *Physical Review Letters*, vol. 17, no. 26, pp. 1286–1289, 1966.

[38] J. Figueroa, Y. Cao, T. Wang, D. Torres, and N. Sepúlveda, "Programming emissivity on fully integrated VO2 windows," *Advanced Materials Letters*, vol. 9, no. 6, pp. 406–410, 2018.

[39] S. Yu, S. Wang, M. Lu, and L. Zuo, "A metal-insulator transition study of VO2 thin films grown on sapphire substrates," *Journal of Applied Physics*, vol. 122, no. 23, p. 235102, 2017.

[40] R. Cabrera, E. Merced, and N. Sepúlveda, "A micro-electro-mechanical memory based on the structural phase transition of $VO_2$," *physica status solidi (a)*, 2013.

[41] Y. Cao, D. Torres, T. Wang, X. Tan, and N. Sepúlveda, "Enabling tunable micromechanical bandpass filters through phase-change materials," *Smart Materials and Structures*, vol. 26, no. 8, p. 085032, 2017.

[42] A. Zaman, A. Alsolami, I. F. Rivera and J. Wang, "Thin-Piezo on Single-Crystal Silicon Reactive Etched RF MEMS Resonators," in *IEEE Access*, vol. 8, pp. 139266-139273, 2020.

[43] D. Torres, T. Wang, J. Zhang, X. Zhang, S. Dooley, X. Tan, H. Xie and N. Sepúlveda, "$VO_2$-Based MEMS Mirrors," *Journal of Microelectromechanical Systems*, vol. 25, no. 4, pp. 780-787, 2016.

[44] N. Sepúlveda, A. Rúa, R. Cabrera, and F. Fernández, "Young's modulus of VO2 thin films as a function of temperature including insulator-to-metal transition regime," *Applied Physics Letters*, vol. 92, no. 19, p. 191913, 2008.

**Ting Hung Liu** (Student Member, IEEE) received his B.S. degree in electrical engineering from Yuan Ze University, Taoyuan, Taiwan in 2014 and his M.S. degree in electrical engineering from University of South Florida, Tampa, FL, USA, in 2018. He is currently pursuing his Ph.D. in Electrical Engineering at the University of South Florida, Tampa, FL advised by Dr. Jing Wang at USF. He participated in 2019 NanoFlorida International Conference to report his work. He served as a Vice Chair of the MTT-S Student Branch Chapter at the University of South Florida in 2020 and he is currently a Chair of the MTT-S Student Branch Chapter at the University of South Florida. He focused on RF MEMS devices specially in piezoelectric resonators research, including design simulation, micro/nanofabrication technologies and power handling measurement.

**Xu Han** received his B.S. degree in Electrical Engineering from University of South Florida in 2014. Prior to that, he was a registered FAA Airframe and Powerplant aircraft maintenance technician. In 2015, he started his Ph.D. program and joined the RF MEMS Transducers Group at USF. His research interests include simulations, designs and micro/nanofabrication technologies for RF MEMS acoustic transducers. He has served as teaching assistants for a number of RF and MEMS related courses, and he also has worked as the lab manager at RF MEMS Transducers Group at USF since 2017. He received his Ph.D. degree in 2021 at University of South Florida, and he is currently a RF filter design engineer at Akoustis Technologies Inc. focusing on many 5G applications.

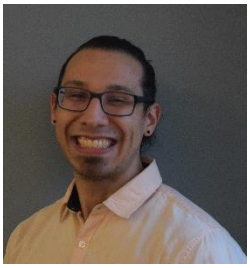

**Juan Pastrana** received his B.S. and M.S. degree in physics from the University of Puerto Rico at Mayagüez, in 2013 and 2017, respectively. He is currently working towards his Ph.D. degree in the Department of Electrical and Computer Engineering at Michigan State University. Previously he worked in the Advanced Materials Dynamics group at the University of Puerto Rico, Mayagüez campus, where he worked in the fabrication and characterization of thin films such as $VO_2$. He has also worked in several research projects at the Air Force Research Laboratories at Wright-Patterson Air Force Base in Dayton, OH. His current research interests include smart materials, and design and fabrication of microelectromechanical systems.

**Nelson Sepulveda** (S'05–M'06–SM'11) received the B.S. degree in electrical and computer engineering from the University of Puerto Rico, Mayagüez, Puerto Rico, in 2001, and the M.S. and Ph.D. degrees in electrical and computer engineering from Michigan State University, East Lansing, MI, USA, in 2002 and 2005, respectively. He has participated in several visiting faculty positions at the National Laboratories. He is currently a Professor with the Electrical and Computer Engineering Department, with a courtesy appointment in the Mechanical Engineering Department, Michigan State University. Prof. Sepúlveda is a recipient of the NSF CAREER (2010), the MSU Teacher-Scholar Award (2015), the Withrow Excellence Awards (2018), and the Marie Sklodowska-Curie Actions Seal of Excellence (2019). His current research is focused on smart materials and their integration in multifunctional devices, flexible piezoelectric/ferroelectret devices, and electromechanical energy-harvesting systems. He is a Senior Member of the IEEE.

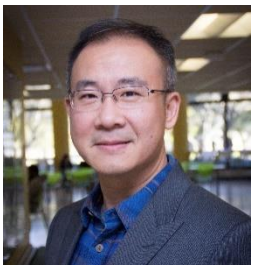

**Jing Wang** (Senior Member, IEEE) received the dual B.S. degrees in mechanical engineering and electrical engineering from Tsinghua University, Beijing, China, in 1994, and the dual M.S. degrees in electrical engineering and mechanical engineering and the Ph.D. degree in electrical engineering from the University of Michigan, Ann Arbor, MI, USA, in 2000, 2002, and 2006, respectively. He joined the University of South Florida, Tampa, FL, USA, in 2006, where he is currently an Agere Systems Endowed Chair in Electrical Engineering.

He has authored or coauthored over 140 professional journal and conference publications. He holds 11 U.S. patents. His current research interests include RF/microwave/devices, advanced additive manufacturing, micromachined transducers, energy scavengers, functional nanomaterials, microfluidics, flexible/RF/microwave electronics, monolithic microwave integrated circuits (MMICs), and wireless sensors.

Dr. Wang was a recipient of the 2018 Faculty Outstanding Research Achievement Award and 2021 Excellence in Innovation Award at the University of South Florida.